Benchmarking Robustness of Adaptation Methods on Pre-trained Vision-Language Models

Shuo Chen[1,3*] **Jindong Gu**[2*] **Zhen Han**[1†] **Yunpu Ma**[1,3] **Philip Torr**[2] **Volker Tresp**[1,4]
[1]Institute of Informatics, LMU Munich [2]Department of Engineering Science, University of Oxford
[3] Siemens AG [4]Munich Center for Machine Learning (MCML)
shuo.chen@campus.lmu.de, jindong.gu@eng.ox.ac.uk, hanzhen02111@163.com

Abstract

Various adaptation methods, such as LoRA, prompts, and adapters, have been proposed to enhance the performance of pre-trained vision-language models in specific domains. As test samples in real-world applications usually differ from adaptation data, studying the robustness of these adaptation methods against distribution shifts is essential. In this study, we assess the robustness of 11 widely-used adaptation methods across 4 vision-language datasets under multimodal corruptions. Concretely, we introduce 7 benchmark datasets, including 96 visual and 87 textual corruptions, to investigate the robustness of different adaptation methods, the impact of available adaptation examples, and the influence of trainable parameter size during adaptation. Our analysis reveals that: 1) Adaptation methods are more sensitive to text corruptions than visual corruptions. 2) Full fine-tuning does not consistently provide the highest robustness; instead, adapters can achieve better robustness with comparable clean performance. 3) Contrary to expectations, our findings indicate that increasing the number of adaptation data and parameters does not guarantee enhanced robustness; instead, it results in even lower robustness. We hope this study could benefit future research in developing robust multimodal adaptation methods. The benchmark, code, and dataset used in this study can be accessed at https://adarobustness.github.io.

1 Introduction

Employing large-scale pre-training of vision-language (VL) models has become the standard for work on VL tasks [38, 70, 39, 71, 70, 2, 71, 77]. These models are typically trained in a self-supervised manner on unlabeled web-scale datasets in a general domain [54, 1]. To address the domain-specific challenges and improve performance on downstream tasks, various model adaptation methods have been proposed [29, 46, 43, 33, 36, 25, 63, 76, 30].

Although adaptation methods can achieve promising results on various VL benchmark datasets, real-world applications often introduce various distribution shifts that differ from the conditions encountered during model adaptation [44]. For instance, these shifts can manifest as variations in lighting conditions in images and typos in texts. Therefore, it is critical to ensure model robustness against distribution shifts, particularly in safety-critical applications where unexpected wrong decisions can have severe consequences, such as self-driving systems [67, 56, 44] and clinical diagnostics [35, 47]. However, robustness research for multimodal models is still rare, leaving many essential questions unanswered: Which adaptation methods perform better on which tasks in terms of both performance and robustness? How robust are the various multimodal adaptation methods against

[*] equal contribution

[†] corresponding author

37th Conference on Neural Information Processing Systems (NeurIPS 2023) Track on Datasets and Benchmarks.

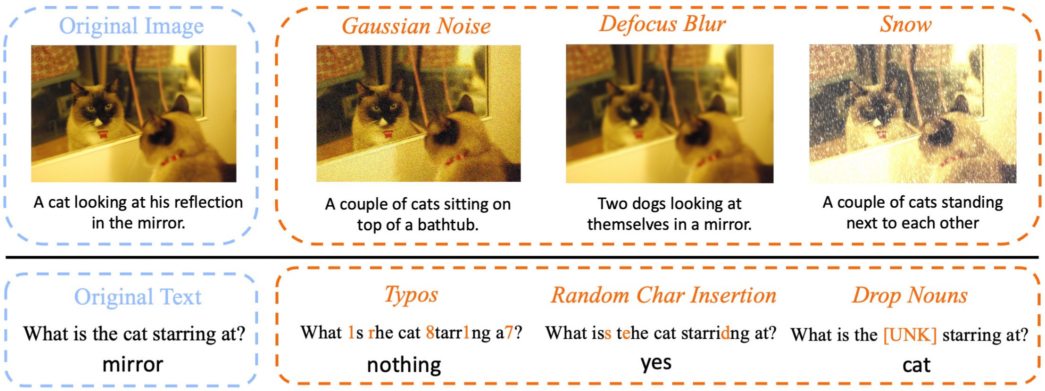
Original Image
A cat looking at his reflection in the mirror.
Gaussian Noise
A couple of cats sitting on top of a bathtub.
Defocus Blur
Two dogs looking at themselves in a mirror.
Snow
A couple of cats standing next to each other
Original Text
What is the cat starring at?
mirror
Typos
What 1s rhe cat 8tarr1ng a7?
nothing
Random Char Insertion
What iss tehe cat starridng at?
yes
Drop Nouns
What is the [UNK] starring at?
cat

Figure 1: Multimodal adaptation methods are sensitive to image and text corruptions. The two rows show image captioning and visual question answering predicted by Adapter [29], respectively. Blue boxes contain the original image and query text. Orange boxes present the corrupted images, texts and model output.

visual corruptions, language corruptions, or both? Will more examples or more trainable parameters assure better robustness?

To this end, this work investigates the robustness of various adaptation methods on VL models to answer the above research questions. Concretely, we introduce a diverse set of 96 visual corruptions, including *impulse noise*, *snow* etc., and 87 textual corruptions encompassing *text addition*, *back translation*, etc. Moreover, extensive experiments have been conducted on 11 adaptation methods across 4 VL datasets, including VQAv2 [20], GQA [31], NLVR^2 [61] and MSCOCO Caption [5]. While several studies have explored the robustness of VL models, our work represents a significant advancement as it provides the first large-scale benchmark robustness analysis of existing adaptation methods on VL models. We limit the models and tasks to those related to images, specifically, multimodal-to-text models, e.g., CLIP-BART [62]. Video-language models are outside the scope of this research.

Our analysis reveals several interesting findings: 1) Adaptation methods demonstrate a higher degree of sensitivity towards text corruptions compared to visual corruptions. 2) Full fine-tuning does not consistently yield the best relative robustness, whereas an adapter can achieve better robustness with comparable performance. 3) Surprisingly, our experiments reveal that a large quantity of adaptation data and model parameters do not guarantee improved robustness. In fact, increasing the amount of adaptation data might even lead to decreased robustness. 4) There is no single adaptation method that surpasses others across all tasks and corruptions. To summarize, our contributions are as follows:

- We construct a suite of 7 large-scale robustness benchmark datasets including 96 visual corruptions and 87 textual corruption methods.
- We evaluate the robustness of 11 adaption methods on VL models based on massive experiments.
- We release the benchmark, code, as well as a leaderboard to the community to facilitate future research on the robustness of multimodal adaptation methods.

2 Related Work

Vision-language Models. Pre-trained VL models [41, 60, 7, 45, 40, 64, 13, 79] have shown outstanding performance on various VL tasks. Some use contrastive learning to align visual features with language representations and achieve surprising zero-shot performance [42, 54]. However, contrastive learning-based methods are limited to close-ended tasks and are inflexible. Another line of work follows BERT's [11] pretrain-then-finetune paradigm [41, 60, 7, 64]. They treat object features extracted using pre-trained object detectors [18] as visual words sent to language models [11]. For example, VL-BART [7] uses BART [37] or T5 [55] as the text encoder and Faster-RCNN [18] as the visual backbone. Unlike other methods, VL-BART unifies VL tasks via a single text generation task. CLIP-BART [62] follows the same idea as VL-BART but adopts the CLIP [54] image encoder to extract pixel-level features. Recent approaches [66, 14, 1] follow such a unified view and freeze large language models (LLMs) to utilize the in-context learning ability of LLMs. However, as shown in [62], LM fine-tuning is still crucial to achieve competitive performance on various downstream VL tasks. In this study, we follow the work in [62] that benchmarks model adaptation methods. CLIP-BART [62] is selected as our VL model, given its generation flexibility and unified architecture.

Model Adaptation Methods. To enhance the performance of pre-trained VL models on downstream tasks and avoid infeasible computation, various adaptation methods have been proposed. Existing methods can be classified into three categories [62]: (1) adding a few trainable parameters while freezing other model parts [29, 46, 43, 33, 36]; (2) updating a few model parameters sparsely [25, 63, 76]; and (3) low-rank factorization of parameters to be updated, such as in LoRA [30]. Adapters [29] belong to the first category and have been widely used in vision, language, and multimodal models [29, 78, 6]. Other representative methods in the first category include Hyperformers [46], Compacters [33], and prompt-tuning [36, 3]. Although numerous adaptation methods have been proposed and widely adopted, their robustness against distribution shifts remains understudied.

Natural Robustness. The robustness of deep learning models against distribution shifts is critical for real-world applications [17, 26, 16]. Regarding vision robustness, researchers have investigated image classification models [26, 16, 28, 57, 21, 22], semantic segmentation [32, 24], object detection [48], video classification [75], and transformer-based architectures [12, 51, 52, 23, 73]. In the field of natural language processing (NLP), many robustness analysis toolboxes [58, 59, 72, 19], and various methods [15, 10, 50, 9] are available. The robustness investigation on multimodal models is gaining more attention but related studies are lacking. The literature includes the robustness of multimodal fusion models [74], audio-visual models [65], text-to-image generative models [8], text-to-video retrieval models [4], as well as image-text models [53].

In contrast to all the works above, our study focuses on *the robustness of adaptation methods integrated into large pre-trained vision-language models*. Understanding their robustness on different VL tasks will facilitate the design of more robust adaptation methods for multimodal models.

3 Preliminaries of Model Adaptation Methods

The pretrain-then-finetune paradigm on large models has shown dominant performance on multimodal tasks [41, 11, 54], yet the prohibitive costs of full fine-tuning have spurred intensive research efforts towards developing parameter-efficient adaptation methods [62, 30, 36, 29, 46, 33]. As the transformer architecture [68] is used for most state-of-the-art large pre-trained models, adaptation methods mainly focus on tweaking the input or the intermediate layers of the attention layers inside the large models. Formally, given a pre-trained large-scale model F parameterized by $\boldsymbol{\theta}$, we need to adapt F on a task-specific dataset $\mathcal{D}$, e.g., a VQA dataset, to get the adapted model F'. Then, we can obtain the output $\mathbf{y} = F'(\mathbf{x}; \boldsymbol{\theta})$ by providing an input $\mathbf{x} = \{x_1, \ldots, x_n\}$ with n tokens from $\mathcal{D}$. Adaptation methods differ in how they interact with $F(\mathbf{x}; \boldsymbol{\theta})$ (Fig. 2). In general, full fine-tuning updates all $\boldsymbol{\theta}$. Prompt [36] concatenates the input $\mathbf{x}$ with an extra prefix. LoRA [30] introduces modifications to the update mechanism of the model parameters $\boldsymbol{\theta}$ and adapters [29, 46, 33] modify the intermediate output and input of $\boldsymbol{\theta}$.

Full fine-tuning directly updates the whole $\boldsymbol{\theta}$ on $\mathcal{D}$ and becomes prohibitive due to the rapidly growing model size. Therefore, the following adaptation methods have been developed to achieve comparable performance while optimizing only a few parameters.

Prompt-based adaptation concatenates the input $\mathbf{x}$ with either a trainable prefix (soft prompt) [36] or a manually designed prefix [3]. For the given input $\mathbf{x} = \{x_1, \ldots, x_n\}$ with n tokens, the pre-trained model will first form an embedding matrix $\mathbf{X} \in \mathbb{R}^{n \times d}$ where d is the dimension of the embedding space. Soft-prompts [36] are then represented as a learnable parameter $\mathbf{P} \in \mathbb{R}^{p \times d}$, where p is the length of the prompt. Next, $\mathbf{P}$ is concatenated with the original embedded input $\mathbf{X}$ to form a new single matrix defined as $[\mathbf{P} \colon \mathbf{X}] \in \mathbb{R}^{(p+n) \times d}$. During adaptation, the model is trained to maximize the probability of the desired output while only updating $\mathbf{P}$.

LoRA [30] utilizes low-rank decomposition matrices to update parameters. For intermediate model parameters $\boldsymbol{\theta}_0 \in \mathbb{R}^{d \times k}$, such as the parameters from a self-attention module in the transformer architecture, its update $\Delta\boldsymbol{\theta}_0$ is represented by a low-rank decomposition $\Delta\boldsymbol{\theta}_0 = \mathbf{BA}, \mathbf{B} \in \mathbb{R}^{d \times r}, \mathbf{A} \in \mathbb{R}^{r \times k}, r \ll min(d, k)$. During adaptation, $\boldsymbol{\theta}_0$ is frozen while $\mathbf{B}$ and $\mathbf{A}$ are updated.

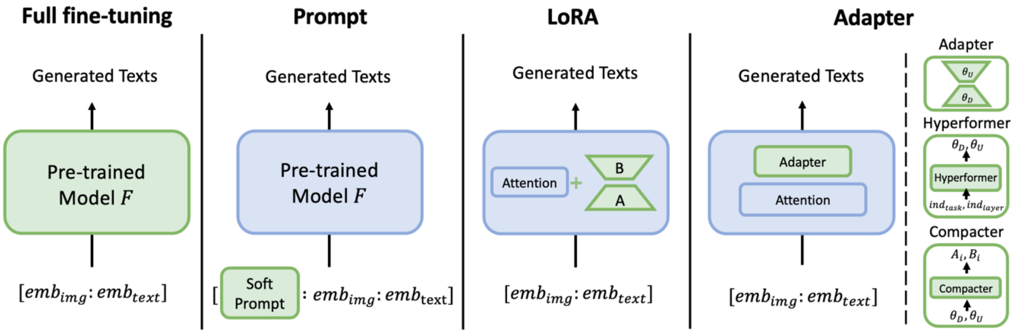

Figure 2: Illustration of adaptation methods used in our study. Green areas indicate trainable parameters whereas frozen parameters are in blue. The input is the concatenation of image and text embedding $[emb_{img} : emb_{text}]$ and the output is the generated text.

Adapter-based adaptation inserts sub-networks with a few learnable parameters into the large model. **Adapter** [29] consists of a pair of downsampling and upsampling layers as well as a residual connection. Suppose the original input to an intermediate layer $\boldsymbol{\theta}_0$ in model F is $\mathbf{x}_0 \in \mathbb{R}^{d_0}$, adapters insert a downsampling layer $\boldsymbol{\theta}^D \in \mathbb{R}^{d_0 \times d_1}$ and an upsampling layer $\boldsymbol{\theta}^{\boldsymbol{U}} \in \mathbb{R}^{d_1 \times d_0}$, where d_0, d_1 are dimensions of the hidden embeddings, respectively. The output after injecting adapters is defined as $\boldsymbol{h} = f_{\boldsymbol{\theta}^U}\left(\sigma\left(f_{\boldsymbol{\theta}^D}(\mathbf{x}_0)\right)\right) + \mathbf{x}_0$, where $f_{\boldsymbol{\theta}^U}$ denotes a function parameterized by $\boldsymbol{\theta}^U$ and $\sigma(\cdot)$ is an activation function such as GELU [27]. To further reduce redundant parameters in adapters, **Compacter** [33] decomposes parameter matrices. It introduces *parameterized hypercomplex multiplication* (PHM) layers $\boldsymbol{\theta}^D = \sum_{i=1}^{k} \mathbf{A}_i \otimes \mathbf{B}_i, \mathbf{A}_i \in \mathbb{R}^{k \times k}, \mathbf{B}_i \in \mathbb{R}^{\frac{d_0}{k} \times \frac{d_1}{k}}$, which decompose the layer in the adapter by Kronecker products. Compacter also shares the parameter of A_i across all layers and decomposes B_i even further with low-rank decomposition. However, as found in [62], such sharing and further decomposition severely decreases the VL performance. In our study, we only use PHM layers. **Hyperformer** [46] relies on a hyper-network shared across tasks to generate the weights in adapters given a task index and a layer index. The hyperformer maintains learnable embeddings for each task and each layer. For N_T tasks and N_L layers, the learnable embeddings in the hyperformer is denoted as $\boldsymbol{t}_1, \ldots, \boldsymbol{t}_{N_T} \in \mathbb{R}^{d_e}$ and $\boldsymbol{l}_1, \ldots, \boldsymbol{l}_{N_L} \in \mathbb{R}^{d_e}$, respectively. The hyperformer consists of a task projector $\boldsymbol{\theta}^T \in \mathbb{R}^{(d_e+d_e) \times d_p}$ and a hyper-network $\boldsymbol{\theta}^H \in \mathbb{R}^{d_p \times (d_0 \times d_1 + d_1 \times d_0)}$, and generates an adapter's weights in the i^{th} layer for the j^{th} task following $\left[\boldsymbol{\theta}^D, \boldsymbol{\theta}^U\right] = f_{\boldsymbol{\theta}^H}\left(f_{\boldsymbol{\theta}^T}\left([\boldsymbol{t}_j, \boldsymbol{l}_i]\right)\right)$.

Adaptation shared over tasks [62] further reduces redundant parameters by exploiting similar information shared across multiple tasks. In a multi-VL-task setting, an intuitive way is to train the adaptation modules per task using: **Multiple Adapters, Multiple Compacters, Multiple LoRA**, and **Multiple Prompts**. Additionally, We can train only one set of adapter layers for all tasks, and we have **Single Adapter, Single Compacter, Single LoRA**, and **Single Prompt**. Besides, **Half-shared adapter** [62] only shares the upsampling layers or downsampling layers across different tasks. Detailed information is presented in Appendix B.2.

4 Corruption Methods

Image Corruptions. We use the corruption methods from ImageNet-C [26] and [4, 53]. A *blank* method is also added, which is used to examine the importance of visual information to VL models. *Blank* corruption turns the original image into a blank picture by setting all pixel values to 255. All image corruptions can be categorized into five groups: **noise**, **blur**, **weather**, **digital**, and **extra**. Specifically, we use 20 image corruption methods, (1) **noise**: *impulse noise, Gaussian noise, shot noise, speckle noise*; (2) **blur**: *zoom blur, defocus blur, motion blur, frosted glass blur, Gaussian blur*; (3) **digital**: *JPEG compression, contrast, elastic, spatter, saturate, pixelate*; (4) **weather**: *snow, frost, fog, brightness*; and (5) **extra**: *blank*. We follow the severity convention in ImageNet-C [26] and define 5 levels of severity for each method, except for *blank* corruption. In total, we have 96 types of visual corruption and we leave the details in the Appendix A.1. By applying all image corruptions to 4 datasets used in this study, i.e., VQAv2 [20], GQA [31], NLVR^2 [61] and MSCOCO Caption [5], we construct 4 out-of-distribution (OOD) benchmark datasets.

Table 1: Dataset Statistics.

	VQAv2		**GQA**		**NLVR^2**		**MSCOCO Caption**	
The Number of	Images	QA pairs	Images	QA pairs	Images	QA pairs	Images	Captions
Training set	113.2K	605.1K	72.1K	943.0K	103.2K	86.4K	113.2K	566.8K
Validation set	5.0K	26.7K	10.2K	132.1K	8.1K	7.0K	5.0K	5.0K
Test set	5.0K	26.3K	398	12.6K	8.1K	7.0K	5.0K	5.0K

Text Corruptions. In addition to visual feature shifts, text corruptions are also essential for evaluating the robustness of vision-language models [4, 53]. We have incorporated a total of 35 corruption methods, inspired by the approaches presented in [72, 53, 4]. These methods can be categorized into three groups based on the level of corruption: **character-level**, **word-level**, and **sentence-level**. Furthermore, they are further subdivided into six sub-categories, namely *character modification, text style modification, text addition, dropping text based on POS, positional drop*, and *text swap*. To name a few examples, the category *text style* transforms sentences to desired styles such as *passive, formal*, or *double negative*. *Text addition* inserts extra words, like adverbs in *InsertAdv*. *Text drop* modifies words based on POS tagging, dropping nouns (*DropNN*) or verbs (*DropVB*). For detailed information, please refer to Appendix A.2 . In addition to the above corruptions, Qiu et al. proposed in [53] that we should ensure that the corrupted text has the same semantics as the original one to make sure the image-text pairs remain meaningful. We follow this setting and use the same fidelity guarantee mechanism as [53]. Various severity levels for text corruptions are also introduced in the benchmark, including 5 severity levels on character-level corruptions and some word-level corruptions. For sentence-level corruptions, only one perturbation is available. In total, we have 87 different perturbations. After applying all text corruptions on VQAv2 [20], GQA [31], and NLVR^2 [61], we construct another 3 OOD benchmark datasets. In the end, we have constructed 7 OOD robustness benchmark datasets to fully investigate the robustness of adaptation methods on vision-language models.

5 Experimental Settings

Tasks and Datasets. The popular representative VL tasks (visual question answering, visual reasoning, and image captioning) and 4 well-known VL datasets are applied in this work. For visual question answering, VQAv2 [20] and GQA [31] are adopted. Additionally, we incorporate NLVR^2 [61] for visual reasoning and MSCOCO [5] for image captioning. The statistics are shown in Table 1.

Models. CLIP-BART (T5) [62] serves as our base model. Because the model adaptation on VL models is mainly on language model components and the encoder-decoder architecture can tackle VL tasks via a unified text-generation task [62]. CLIP-BART (T5) utilizes a single-stream fusion scheme, where the language model takes the concatenation of visual representations and text representations as input. The single-stream approach enables the model to effectively integrate visual and textual information, leveraging the complementary strengths of both modalities. Specifically, CLIP-ResNet101 [54] is the vision encoder that receives resized 224×224 images, and representations from the last convolutional layer are extracted as the visual features. BART$_{base}$ [37] and T5$_{base}$ [55] deal with the downstream text generation task.

Model Adaptation Methods. We investigate the robustness of four mainstream adaptation methods: full fine-tuning, soft prompt [36], LoRA [30], and adapter-based methods, including Adapter [29], Hyperformer [46], and Compacter [33]. To better understand their robustness, shared adaptation methods are also investigated. Specifically, for soft prompt, i.e., LoRA, and Compacters, we conduct experiments in both single and multiple manners and the half-shared manner for Adapter (Section 3). See Appendix B.2 for detailed information, e.g., training strategy and hyperparameters.

VL Task Evaluation Metrics. Accuracy on the Karpathy-test split is evaluated for VQAv2. For GQA, accuracy on the test-dev split is evaluated, and accuracy on the test-P split is used for NLVR^2. In image captioning, we use CIDEr [69] on the Karpathy-test split.

Robustness Evaluation Protocol. The model performance P_I on D_I (i.e., in-distribution test datasets) and P_O on D_O (i.e., out-of-distribution test datasets) are first evaluated, where P is the corresponding evaluation metric for each task, such as CIDEr [69] for image caption. Then, the

Table 2: Clean performance and relative robustness (RR) of adaptation methods based on CLIP-BART against image (up) and text (down) corruptions. RR and the corresponding standard deviation are averaged and calculated over all image or text corruption methods. The percentage of trainable parameters for each adaptation method is also reported. We strike out those high RRs with quite low performance. The best RR for each column is in bold.

Adaptation method	Updated	**VQAv2**		**GQA**		**NLVR^2**		**MSCOCO Caption**	
Image Corruptions	Params	Acc (%)	RR (%)	Acc (%)	RR (%)	Acc (%)	RR (%)	CIDEr	RR (%)
Full Fine-tuning	100%	66.75	84.86±5.17	55.04	89.20±0.04	73.01	90.34±0.04	115.03	68.40±0.14
Multiple Adapters	12.22%	65.30	85.33±4.90	53.39	86.16±0.04	69.41	**92.02**±0.04	114.47	68.72±0.14
Half-shared Adapters	8.36%	65.20	85.18±5.01	52.96	89.37±0.04	70.03	91.72±0.04	114.50	68.45±0.14
Single Adapter	4.18%	65.35	**85.76**±5.32	54.14	82.49±0.04	73.89	90.04±0.05	115.04	68.68±0.14
Hyperformer	5.79%	65.38	85.38±4.84	52.52	90.05±0.04	72.21	90.13±0.05	114.89	68.74±0.14
Multiple Compacters	7.05%	64.91	85.65±4.81	52.75	88.89±0.04	69.45	91.33±0.04	115.16	68.67±0.13
Single Compacter	2.70%	64.47	85.47±4.96	52.90	82.62±0.04	69.94	92.04±0.04	113.06	**69.92**±0.13
Multiple LoRA	17.72%	65.44	84.78±4.86	52.05	**91.15**±0.04	51.32	–	115.41	68.47±0.14
Single LoRA	5.93%	65.34	84.78±4.81	53.19	82.58±0.04	73.58	90.05±0.04	114.54	69.26±0.13
Multiple Prompts	4.53%	46.81	–	34.01	–	49.87	–	108.62	67.70±0.14
Single Prompt	2.00%	44.00	–	37.54	–	51.95	–	103.70	68.56±0.13

Adaptation method	Updated	**VQAv2**		**GQA**		**NLVR^2**	
Text Corruptions	Params	Acc (%)	RR (%)	Acc (%)	RR (%)	Acc (%)	RR (%)
Full Fine-tuning	100%	66.75	73.65±22.38	55.04	66.92±24.14	73.01	87.06±11.00
Multiple Adapters	12.22%	65.30	76.62±20.66	53.39	66.93±22.43	69.41	**90.14**±10.19
Half-shared Adapters	8.36%	65.20	76.78±20.79	52.96	68.20±24.78	70.03	89.16±10.12
Single Adapter	4.18%	65.35	**77.64**±21.09	54.14	67.47±20.03	73.89	88.49±10.87
Hyperformer	5.79%	65.38	75.06±21.29	52.52	**70.30**±23.13	72.21	87.27±11.27
Multiple Compacters	7.05%	64.91	77.10±20.85	52.75	67.39±23.29	69.45	90.00±9.76
Single Compacter	2.70%	64.47	77.17±20.40	52.90	67.90±20.33	69.94	90.10±9.81
Multiple LoRA	17.72%	65.44	74.04±21.97	52.05	68.77±22.76	51.32	–
Single LoRA	5.93%	65.34	74.50±21.42	53.19	63.94±20.99	73.58	87.64±11.04
Multiple Prompts	4.53%	46.81	–	34.01	–	49.87	–
Single Prompt	2.00%	44.00	–	37.54	–	51.95	–

Relative Robustness $RR = 1 - \Delta P / P_I$ [53, 4] is computed based on the clean performance P_I and corrupted performance P_O, where $\Delta P = (P_I - P_O)$. RR is a score ranging from 0 to 1, where $RR = 1$ indicates that F is totally robust and $R = 0$ means that F is not robust at all. The RR with severity 5 is reported across the main paper; detailed scores on others are in Supplementary.

6 Results and Analysis

Sec. 6.1 examines the robustness of each adaptation method and tries to answer the first question: *Which adaptation methods perform better on which tasks with respect to both performance and robustness?* Sec. 6.2 compares the robustness sensitivity on image and text corruptions and looks for the answer to *how robust are the various multimodal adaptation methods against visual corruptions, language corruptions, or both?* In Section 6.3, we analyze the influence on robustness given different sizes of adaptation data and trainable parameters. Especially, we aim to answer *will more examples or more parameters ensure better adaptation robustness?*

6.1 Robustness of Multimodal Adaptation Methods

Full fine-tuning, prompt-tuning, LoRA, and adapter-based methods are four types of adaptation methods investigated in this study, and their relative robustness against image and text corruptions are presented in Table 2 .The reported relative robustness is the average value across all images or text corruption methods. **Although full fine-tuning generally achieves higher clean performance, our analysis reveals that its robustness is comparatively weaker than other adaptation methods.** In many cases, the adapter and hyperformer achieve better robustness with much fewer parameters and comparable clean performance. For instance, full fine-tuning's RR against text corruptions on the VQAv2 dataset is the smallest, for both CLIP-BART and CLIP-T5. Prompt tuning, despite exhibiting high robustness, fails to perform well on the clean test dataset. The same conclusions can be drawn on corrupted data with different corruption levels, as shown in Supplementary. Please note that we have excluded robustness scores associated with very low task performance in Table 2.

Single Adapter vs Full Fine-tuning. Previous research [62] has shown that a single adapter can achieve comparable performance on the four tasks with significantly fewer parameters than full fine-tuning. When it comes to robustness, *a single adapter is comparable to or slightly better than full fine-tuning on VQAv2, NLVR^2, and MSCOCO Caption given image corruptions.* The same goes for text corruption. For example, as shown in the 4th row and 1st row in Table 2 (lower panel), a single adapter on CLIP-BART achieves an average RR of 77.64% against text corruptions on VQAv2, while full fine-tuning's RR is 73.65%. However, on GQA, a single adapter is less robust than full fine-tuning. Full fine-tuning achieves an average RR of 89.20% against image corruptions, while the RR of a single adapter is only 82.49%. Also, a single adapter's clean accuracy on GQA is lower than full fine-tuning's 55.04%. In contrast, multiple and half-shared adapters have more parameters but achieve better robustness on the four tasks than a single adapter. **In conclusion, a single adapter can achieve similar or better robustness on VQAv2, NLVR^2, and MSCOCO Caption compared to full fine-tuning. On GQA, multiple and half-shared adapters are better.**

Adapter-based Methods. Although training multiple tasks with one set of adapter layers has the least number of parameters, *such a single setting might hinder the robustness on certain tasks*. For instance, Single Adapter's robustness on GQA against image corruptions (82.49%) is lower than that of the half-shared (89.37%) and multiple settings (86.16%). This also applies to Single LoRA and Single Compacter. An explanation could be that the half-shared mechanism does not only learn more general representation across tasks; it also maintains task-specific knowledge. On GQA, Single LoRA's robustness against image corruptions is lower by 8.57% compared to Multiple LoRA's, and the robustness against text corruptions is lower by 4.83%. However, compared with multiple settings of LoRA and Adapter, the *Hyperformer has relatively fewer parameters but achieves comparable or better robustness*. Hyperformer on CLIP-T5 also obtains the best robustness results against image corruptions on all four tasks.

Robustness against Natural Dataset Distribution Shift. To provide a more realistic assessment of the robustness, an additional natural distribution shift corruption is included in our work. VQA-RAD [34] is a manually constructed dataset where clinicians asked naturally occurring questions about radiology images and provided reference answers. The images in VQA-RAD are shown neither in model pre-training nor in adaptation and can be seen as a natural out-of-distribution dataset. Results in Fig. 3 are relatively low but adapters perform relatively well, such as the Single Adapter in CLIP-BART and Multiple Adapters in CLIP-T5. Full finetuning fails to generalize well in CLIP-BART compared to other adaptation methods whereas the performance of CLIP-T5 with full finetuning is the second best.

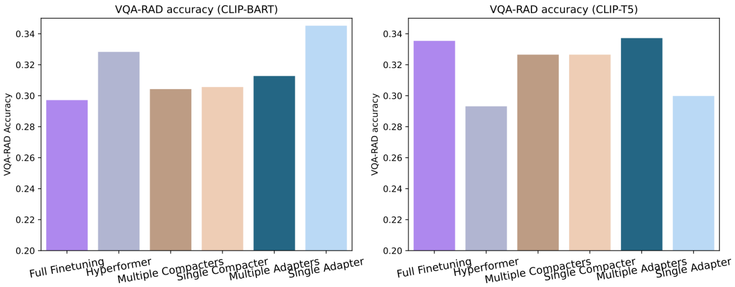

Figure 3: The accuracy results on VQA-RAD [34] which include 11 adaptation methods on CLIP-BART (left) and 6 on CLIP-T5 (right).

Vision-language Tasks. Among all datasets, MSCOCO Caption is the most vulnerable one against image corruptions, where all adaptation methods have decreased on average more than 30%. This is plausible as it only relies on visual information, whereas other tasks provide both visual and language information. Besides, GQA is the task with the lowest robustness performance against text corruptions. Moreover, *on GQA, the extreme single-module setting fails to achieve good robustness*, such as Single Adapter, Single LoRA, and Single Compacter. **This indicates that information sharing with the other two datasets may hinder the robustness on GQA.** To overcome such an issue, one can adopt the multiple-module manner or Hyperformer. Adaptation methods show better robustness on NLVR^2 compared to the other three tasks on both corruptions.

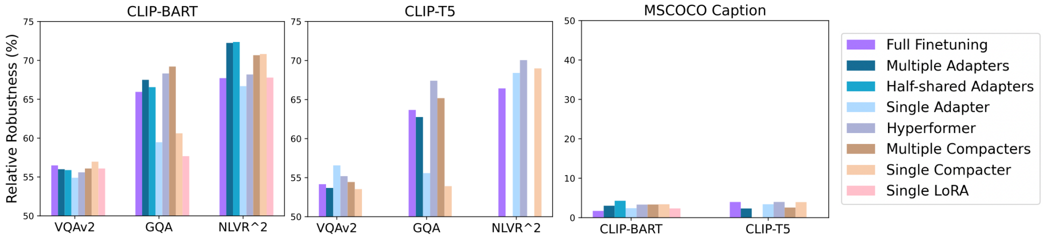

Figure 4: Relative robustness (%) of adaptation methods based on CLIP-BART (left) and CLIP-T5 (middle) against *blank* corruption. We group MSCOCO Caption results from CLIP-BART and CLIP-T5 together in the right sub-figure. We omit two bars in NLVR^2 from the middle figure as multiple adapters and multiple compacters did not perform well.

6.2 Robustness Sensitivity to Image Corruptions and Text Corruptions

This work introduces both image and text corruptions to examine the robustness of various adaptation methods. **Our experimental findings suggest a potential vulnerability of adaptation methods on multimodal VL models to text corruptions, particularly those at the character level**. Across all three tasks, the adaptation methods exhibit lower robustness indicators against text corruptions. For instance, Single Adapter based on CLIP-BART has the best robustness result of 85.76% against image corruptions on VQAv2. However, although it is still the most robust adaptation method against text corruptions, the relative robustness is 77.64%. *Among image corruptions, zoom blur drops the robustness the most, and within text corruptions, char-level methods are most challenging to these VL adaptation methods*. Detailed analysis is in Supplementary Section 6.

Blank Image Corruption. *Blank* corruption evaluates the influence on the robustness of visual information in VL tasks. All datasets used in this study rely on visual information and only the MSCOCO Caption contains no language information. In *blank* corruption, we set the pixel values of testing image data to 255, i.e. transforming the original image into a blank image. The results are shown in Fig. 4. The relative robustness on MSCOCO Caption is the lowest among all four datasets. This is plausible since image captioning relies only on visual information and is not supposed to perform well given a blank image. Apart from image captioning, adaptation methods on all three datasets could secure relative robustness exceeding 50% in the absence of useful visual information. Several questions within the VL tasks can be accurately answered without relying on visual information, suggesting that **language information plays a more significant role than visual information**. This also explains the higher sensitivity to text perturbations compared to the sensitivity to image corruptions.

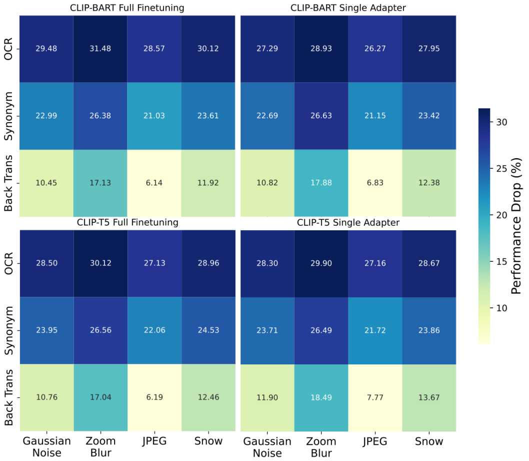

Figure 5: The average performance drop given both visual and text corruptions. A darker color indicates a severe performance drop.

Compounding Effects of Multimodal Corruptions. To assess the impact of compounding distribution shifts on both the visual and text modalities, we selected a subset of corruption methods from each category and presented the results in Fig. 5. Specifically, for text corruption methods, we selected *ocr* at the character level, *swap syn word embd* at the word level, and *back translation* at the sentence level. For visual corruption methods, we selected *Gaussian noise* in the noise category, *zoom blur* in the blur category, *JPEG* in the digital category, and *snow* in the weather category. We tested the full finetuning and single adapter on CLIP-BART and CLIP-T5. The results demonstrate that combining corruptions from two modalities can lead to a greater drop in robustness. Additionally, the results show similar trends as the single-modal corruptions. Character-level corruptions still lead to the most severe performance drop compared

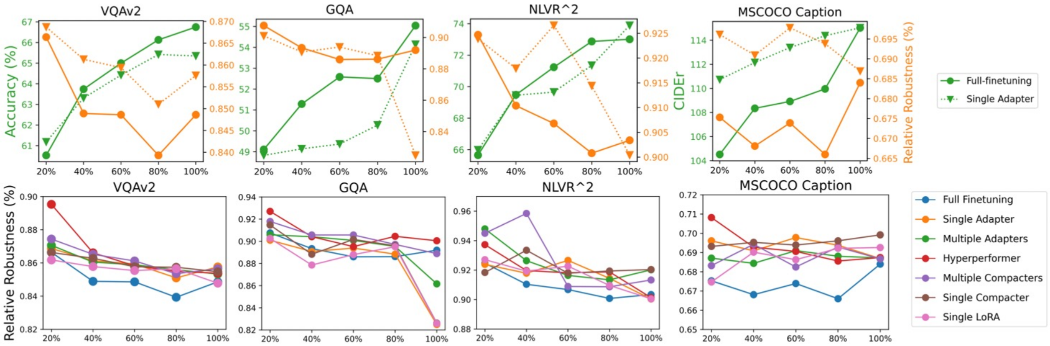

Figure 6: The first row represents the clean performance and relative robustness of full fine-tuning and single adapter on CLIP-BART given the different sizes of the adaptation dataset. Green lines stand for performance in each task and the orange is robustness. The second row is relative robustness given the different sizes of the adaptation dataset. The X-axis shows the random subset ratio of the training dataset during adaptation, ranging from 20% to 100%.

to sentence- and word-level corruptions. *Zoom blur* still drops the robustness the most among image corruptions.

6.3 The Influence of Adaptation Data Size and Parameter Size on Robustness

Adaptation Data Size. Adaptation methods are gaining more attention due to their efficient fine-tuning manner compared to full fine-tuning. We take a further step and evaluate their performance and robustness given different sizes of training data during adaptation. Fig. 6 compares the performance and robustness of full fine-tuning and single adapter. Given more adaptation data, performance in all tasks has a steady increase, and in most cases, the performance of full fine-tuning surpasses single adapter's performance, while the latter can achieve comparable performance given the whole adaptation data. Only on MSCOCO Caption, single adapter outperforms full fine-tuning given a subset of adaptation data. Single adapter achieves better RR compared to full fine-tuning against both image and text corruptions but has a robustness drop on GQA. Fig. 6 also demonstrates the robustness of other adaptation methods. All lines present a steady declining tendency, which indicates that **increasing the size of the adaptation data does not consistently enhance relative robustness**. Besides, the blue full fine-tuning lines take the lowest position on all three datasets given text corruptions and on VQAv2, NLVR^2, and MSCOCO Caption given image corruptions. In comparison to other adaptation methods, *full fine-tuning has relatively lower relative robustness, despite having the most trainable parameters*. The last conclusion is that **there is no single adaptation method that surpasses others across all tasks and corruptions** and all methods share a similar robustness fluctuation given a different size of the adaptation dataset.

Adaptation Parameter Size. Fig. 7 presents RR and clean performance of prompt-tuning given different soft prompt lengths added to the concatenated embeddings. There is a steady increase in the performance on four tasks with longer prompt lengths which proves that prompt methods perform better given more parameters. Regarding relative robustness, such a steady increase does not apply to all tasks, and **longer soft prompts do not ensure better relative robustness**. Fig. 7 also shows the experimental results from the other 4 adaptation methods given different sizes of trainable parameters. The results demonstrate that **more parameters do not ensure enhanced robustness and some even reduce it**, such as the single compacter and single adapter on GQA.

7 Discussion and Conclusion

This study focuses on the robustness of adaptation methods on pre-trained vision-language models and provides 7 benchmark datasets containing 96 visual and 87 textual corruptions. We systematically inspect the robustness of 11 adaptation methods on 4 popular VL datasets and conclude that: 1) these adaptation methods are more sensitive towards text corruptions compared to visual corruptions, 2) full fine-tuning does not achieve the best robustness; instead, adapters demonstrate better robustness while maintaining comparable performance, 3) surprisingly, more adaptation data and more parameters do

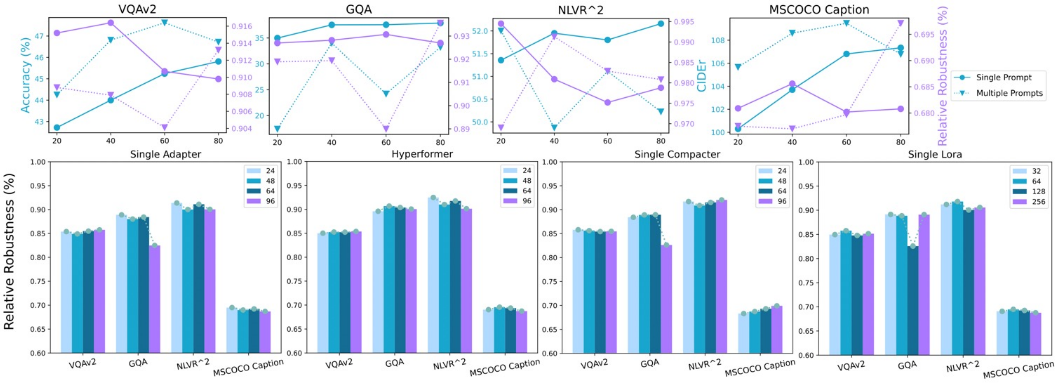

Figure 7: The top row shows the clean performance and relative robustness from prompt adaptations with different prompt lengths on CLIP-BART. Blue lines stand for performance on each task and purple lines represent relative robustness. The bottom row shows the relative robustness given the different number of parameters in 4 adaptation methods. Different colors stand for different embedding sizes and larger numbers are with more parameters.

not ensure a better robustness. In fact, it can even lead to worse robustness, 4) there is currently no adaptation method achieving both the best performance and best robustness across all corruptions and all tasks. The main limitation of this work is that the analysis is on a limited number of multimodal models due to the availability of usable code, model weights, and massive experiments. Potential future work includes investigating more diverse pre-trained VL models, designing more robust adaptation methods, and integrating future model adaptation methods to make our benchmark up-to-date.

Acknowledgments and Disclosure of Funding

This work is partially supported by the UKRI grant: Turing AI Fellowship EP/W002981/1 and EPSRC/MURI grant: EP/N019474/1. We would also like to thank the Royal Academy of Engineering and FiveAI. We also gratefully acknowledge the computational and data resources provided by the Leibniz Supercomputing Centre (www.lrz.de).

References

[1] Jean-Baptiste Alayrac, Jeff Donahue, Pauline Luc, Antoine Miech, Iain Barr, Yana Hasson, Karel Lenc, Arthur Mensch, Katherine Millican, Malcolm Reynolds, et al. Flamingo: a visual language model for few-shot learning. *Advances in Neural Information Processing Systems*, 35:23716–23736, 2022.

[2] Hangbo Bao, Wenhui Wang, Li Dong, Qiang Liu, Owais Khan Mohammed, Kriti Aggarwal, Subhojit Som, Songhao Piao, and Furu Wei. Vlmo: Unified vision-language pre-training with mixture-of-modality-experts. *Advances in Neural Information Processing Systems*, 35:32897–32912, 2022.

[3] Tom Brown, Benjamin Mann, Nick Ryder, Melanie Subbiah, Jared D Kaplan, Prafulla Dhariwal, Arvind Neelakantan, Pranav Shyam, Girish Sastry, Amanda Askell, et al. Language models are few-shot learners. *Advances in neural information processing systems*, 33:1877–1901, 2020.

[4] Madeline Chantry, Shruti Vyas, Hamid Palangi, Yogesh Rawat, and Vibhav Vineet. Robustness analysis of video-language models against visual and language perturbations. *Advances in Neural Information Processing Systems*, 35:34405–34420, 2022.

[5] Xinlei Chen, Hao Fang, Tsung-Yi Lin, Ramakrishna Vedantam, Saurabh Gupta, Piotr Dollár, and C Lawrence Zitnick. Microsoft coco captions: Data collection and evaluation server. *arXiv preprint arXiv:1504.00325*, 2015.

[6] Zhe Chen, Yuchen Duan, Wenhai Wang, Junjun He, Tong Lu, Jifeng Dai, and Yu Qiao. Vision transformer adapter for dense predictions. *arXiv preprint arXiv:2205.08534*, 2022.

[7] Jaemin Cho, Jie Lei, Hao Tan, and Mohit Bansal. Unifying vision-and-language tasks via text generation. In *International Conference on Machine Learning*, pages 1931–1942. PMLR, 2021.

[8] Jaemin Cho, Abhay Zala, and Mohit Bansal. Dall-eval: Probing the reasoning skills and social biases of text-to-image generative transformers. *arXiv preprint arXiv:2202.04053*, 2022.

[9] Maria De-Arteaga, Alexey Romanov, Hanna Wallach, Jennifer Chayes, Christian Borgs, Alexandra Chouldechova, Sahin Geyik, Krishnaram Kenthapadi, and Adam Tauman Kalai. Bias in bios: A case study of semantic representation bias in a high-stakes setting. In *proceedings of the Conference on Fairness, Accountability, and Transparency*, pages 120–128, 2019.

[10] Dorottya Demszky, Devyani Sharma, Jonathan H Clark, Vinodkumar Prabhakaran, and Jacob Eisenstein. Learning to recognize dialect features. *arXiv preprint arXiv:2010.12707*, 2020.

[11] Jacob Devlin, Ming-Wei Chang, Kenton Lee, and Kristina Toutanova. Bert: Pre-training of deep bidirectional transformers for language understanding. *arXiv preprint arXiv:1810.04805*, 2018.

[12] Alexey Dosovitskiy, Lucas Beyer, Alexander Kolesnikov, Dirk Weissenborn, Xiaohua Zhai, Thomas Unterthiner, Mostafa Dehghani, Matthias Minderer, Georg Heigold, Sylvain Gelly, et al. An image is worth 16x16 words: Transformers for image recognition at scale. *arXiv preprint arXiv:2010.11929*, 2020.

[13] Yifan Du, Zikang Liu, Junyi Li, and Wayne Xin Zhao. A survey of vision-language pre-trained models. *arXiv preprint arXiv:2202.10936*, 2022.

[14] Constantin Eichenberg, Sidney Black, Samuel Weinbach, Letitia Parcalabescu, and Anette Frank. Magma–multimodal augmentation of generative models through adapter-based finetuning. *arXiv preprint arXiv:2112.05253*, 2021.

[15] Matt Gardner, Yoav Artzi, Victoria Basmova, Jonathan Berant, Ben Bogin, Sihao Chen, Pradeep Dasigi, Dheeru Dua, Yanai Elazar, Ananth Gottumukkala, et al. Evaluating models' local decision boundaries via contrast sets. *arXiv preprint arXiv:2004.02709*, 2020.

[16] Robert Geirhos, Patricia Rubisch, Claudio Michaelis, Matthias Bethge, Felix A Wichmann, and Wieland Brendel. Imagenet-trained cnns are biased towards texture; increasing shape bias improves accuracy and robustness. *arXiv preprint arXiv:1811.12231*, 2018.

[17] Robert Geirhos, Carlos RM Temme, Jonas Rauber, Heiko H Schütt, Matthias Bethge, and Felix A Wichmann. Generalisation in humans and deep neural networks. *Advances in neural information processing systems*, 31, 2018.

[18] Ross Girshick. Fast r-cnn. In *Proceedings of the IEEE international conference on computer vision*, pages 1440–1448, 2015.

[19] Karan Goel, Nazneen Rajani, Jesse Vig, Samson Tan, Jason Wu, Stephan Zheng, Caiming Xiong, Mohit Bansal, and Christopher Ré. Robustness gym: Unifying the nlp evaluation landscape. *arXiv preprint arXiv:2101.04840*, 2021.

[20] Yash Goyal, Tejas Khot, Douglas Summers-Stay, Dhruv Batra, and Devi Parikh. Making the v in vqa matter: Elevating the role of image understanding in visual question answering. In *Proceedings of the IEEE conference on computer vision and pattern recognition*, pages 6904–6913, 2017.

[21] Jindong Gu and Volker Tresp. Improving the robustness of capsule networks to image affine transformations. In *Proceedings of the IEEE/CVF Conference on Computer Vision and Pattern Recognition*, pages 7285–7293, 2020.

[22] Jindong Gu, Volker Tresp, and Han Hu. Capsule network is not more robust than convolutional network. In *Proceedings of the IEEE/CVF Conference on Computer Vision and Pattern Recognition*, pages 14309–14317, 2021.

[23] Jindong Gu, Volker Tresp, and Yao Qin. Are vision transformers robust to patch perturbations? In *Computer Vision–ECCV 2022: 17th European Conference, Tel Aviv, Israel, October 23–27, 2022, Proceedings, Part XII*, pages 404–421. Springer, 2022.

[24] Jindong Gu, Hengshuang Zhao, Volker Tresp, and Philip HS Torr. Segpgd: An effective and efficient adversarial attack for evaluating and boosting segmentation robustness. In *Computer Vision–ECCV 2022: 17th European Conference, Tel Aviv, Israel, October 23–27, 2022, Proceedings, Part XXIX*, pages 308–325. Springer, 2022.

[25] Demi Guo, Alexander M Rush, and Yoon Kim. Parameter-efficient transfer learning with diff pruning. *arXiv preprint arXiv:2012.07463*, 2020.

[26] Dan Hendrycks and Thomas Dietterich. Benchmarking neural network robustness to common corruptions and perturbations. *arXiv preprint arXiv:1903.12261*, 2019.

[27] Dan Hendrycks and Kevin Gimpel. Bridging nonlinearities and stochastic regularizers with gaussian error linear units. *CoRR, abs/1606.08415*, 3, 2016.

[28] Dan Hendrycks, Kevin Zhao, Steven Basart, Jacob Steinhardt, and Dawn Song. Natural adversarial examples. In *Proceedings of the IEEE/CVF Conference on Computer Vision and Pattern Recognition*, pages 15262–15271, 2021.

[29] Neil Houlsby, Andrei Giurgiu, Stanislaw Jastrzebski, Bruna Morrone, Quentin De Laroussilhe, Andrea Gesmundo, Mona Attariyan, and Sylvain Gelly. Parameter-efficient transfer learning for nlp. In *International Conference on Machine Learning*, pages 2790–2799. PMLR, 2019.

[30] Edward J Hu, Yelong Shen, Phillip Wallis, Zeyuan Allen-Zhu, Yuanzhi Li, Shean Wang, Lu Wang, and Weizhu Chen. Lora: Low-rank adaptation of large language models. *arXiv preprint arXiv:2106.09685*, 2021.

[31] Drew A Hudson and Christopher D Manning. Gqa: A new dataset for real-world visual reasoning and compositional question answering. In *Proceedings of the IEEE/CVF conference on computer vision and pattern recognition*, pages 6700–6709, 2019.

[32] Christoph Kamann and Carsten Rother. Benchmarking the robustness of semantic segmentation models. In *Proceedings of the IEEE/CVF conference on computer vision and pattern recognition*, pages 8828–8838, 2020.

[33] Rabeeh Karimi Mahabadi, James Henderson, and Sebastian Ruder. Compacter: Efficient low-rank hypercomplex adapter layers. *Advances in Neural Information Processing Systems*, 34:1022–1035, 2021.

[34] Jason J Lau, Soumya Gayen, Asma Ben Abacha, and Dina Demner-Fushman. A dataset of clinically generated visual questions and answers about radiology images. *Scientific data*, 5(1):1–10, 2018.

[35] Joonsang Lee, Angela Steinmann, Yao Ding, Hannah Lee, Constance Owens, Jihong Wang, Jinzhong Yang, David Followill, Rachel Ger, Dennis MacKin, et al. Radiomics feature robustness as measured using an mri phantom. *Scientific reports*, 11(1):3973, 2021.

[36] Brian Lester, Rami Al-Rfou, and Noah Constant. The power of scale for parameter-efficient prompt tuning. *arXiv preprint arXiv:2104.08691*, 2021.

[37] Mike Lewis, Yinhan Liu, Naman Goyal, Marjan Ghazvininejad, Abdelrahman Mohamed, Omer Levy, Ves Stoyanov, and Luke Zettlemoyer. Bart: Denoising sequence-to-sequence pre-training for natural language generation, translation, and comprehension. *arXiv preprint arXiv:1910.13461*, 2019.

[38] Chenliang Li, Haiyang Xu, Junfeng Tian, Wei Wang, Ming Yan, Bin Bi, Jiabo Ye, Hehong Chen, Guohai Xu, Zheng Cao, et al. mplug: Effective and efficient vision-language learning by cross-modal skip-connections. *arXiv preprint arXiv:2205.12005*, 2022.

[39] Junnan Li, Dongxu Li, Silvio Savarese, and Steven Hoi. Blip-2: Bootstrapping language-image pre-training with frozen image encoders and large language models. *arXiv preprint arXiv:2301.12597*, 2023.

[40] Junnan Li, Ramprasaath Selvaraju, Akhilesh Gotmare, Shafiq Joty, Caiming Xiong, and Steven Chu Hong Hoi. Align before fuse: Vision and language representation learning with momentum distillation. *Advances in neural information processing systems*, 34:9694–9705, 2021.

[41] Liunian Harold Li, Mark Yatskar, Da Yin, Cho-Jui Hsieh, and Kai-Wei Chang. Visualbert: A simple and performant baseline for vision and language. *arXiv preprint arXiv:1908.03557*, 2019.

[42] Wei Li, Can Gao, Guocheng Niu, Xinyan Xiao, Hao Liu, Jiachen Liu, Hua Wu, and Haifeng Wang. Unimo: Towards unified-modal understanding and generation via cross-modal contrastive learning. *arXiv preprint arXiv:2012.15409*, 2020.

[43] Xiang Lisa Li and Percy Liang. Prefix-tuning: Optimizing continuous prompts for generation. *arXiv preprint arXiv:2101.00190*, 2021.

[44] Ze Liu, Yingfeng Cai, Hai Wang, Long Chen, Hongbo Gao, Yunyi Jia, and Yicheng Li. Robust target recognition and tracking of self-driving cars with radar and camera information fusion under severe weather conditions. *IEEE Transactions on Intelligent Transportation Systems*, 23(7):6640–6653, 2021.

[45] Jiasen Lu, Dhruv Batra, Devi Parikh, and Stefan Lee. Vilbert: Pretraining task-agnostic visiolinguistic representations for vision-and-language tasks. *Advances in neural information processing systems*, 32, 2019.

[46] Rabeeh Karimi Mahabadi, Sebastian Ruder, Mostafa Dehghani, and James Henderson. Parameter-efficient multi-task fine-tuning for transformers via shared hypernetworks. *arXiv preprint arXiv:2106.04489*, 2021.

[47] Joscha Maier, Elias Eulig, Tim Vöth, Michael Knaup, Jan Kuntz, Stefan Sawall, and Marc Kachelrieß. Real-time scatter estimation for medical ct using the deep scatter estimation: Method and robustness analysis with respect to different anatomies, dose levels, tube voltages, and data truncation. *Medical physics*, 46(1):238–249, 2019.

[48] Claudio Michaelis, Benjamin Mitzkus, Robert Geirhos, Evgenia Rusak, Oliver Bringmann, Alexander S Ecker, Matthias Bethge, and Wieland Brendel. Benchmarking robustness in object detection: Autonomous driving when winter is coming. *arXiv preprint arXiv:1907.07484*, 2019.

[49] George A Miller. Wordnet: a lexical database for english. *Communications of the ACM*, 38(11):39–41, 1995.

[50] John Miller, Karl Krauth, Benjamin Recht, and Ludwig Schmidt. The effect of natural distribution shift on question answering models. In *International Conference on Machine Learning*, pages 6905–6916. PMLR, 2020.

[51] Sayak Paul and Pin-Yu Chen. Vision transformers are robust learners. In *Proceedings of the AAAI Conference on Artificial Intelligence*, volume 36, pages 2071–2081, 2022.

[52] Francesco Pinto, Philip HS Torr, and Puneet K. Dokania. An impartial take to the cnn vs transformer robustness contest. In *Computer Vision–ECCV 2022: 17th European Conference, Tel Aviv, Israel, October 23–27, 2022, Proceedings, Part XIII*, pages 466–480. Springer, 2022.

[53] Jielin Qiu, Yi Zhu, Xingjian Shi, Florian Wenzel, Zhiqiang Tang, Ding Zhao, Bo Li, and Mu Li. Are multimodal models robust to image and text perturbations? *arXiv preprint arXiv:2212.08044*, 2022.

[54] Alec Radford, Jong Wook Kim, Chris Hallacy, Aditya Ramesh, Gabriel Goh, Sandhini Agarwal, Girish Sastry, Amanda Askell, Pamela Mishkin, Jack Clark, et al. Learning transferable visual models from natural language supervision. In *International conference on machine learning*, pages 8748–8763. PMLR, 2021.

[55] Colin Raffel, Noam Shazeer, Adam Roberts, Katherine Lee, Sharan Narang, Michael Matena, Yanqi Zhou, Wei Li, and Peter J Liu. Exploring the limits of transfer learning with a unified text-to-text transformer. *The Journal of Machine Learning Research*, 21(1):5485–5551, 2020.

[56] Julien Rebut, Andrei Bursuc, and Patrick Pérez. Styleless layer: Improving robustness for real-world driving. In *2021 IEEE/RSJ International Conference on Intelligent Robots and Systems (IROS)*, pages 8992–8999. IEEE, 2021.

[57] Benjamin Recht, Rebecca Roelofs, Ludwig Schmidt, and Vaishaal Shankar. Do imagenet classifiers generalize to imagenet? In *International conference on machine learning*, pages 5389–5400. PMLR, 2019.

[58] Marco Tulio Ribeiro, Tongshuang Wu, Carlos Guestrin, and Sameer Singh. Beyond accuracy: Behavioral testing of nlp models with checklist. *arXiv preprint arXiv:2005.04118*, 2020.

[59] Barbara Rychalska, Dominika Basaj, Alicja Gosiewska, and Przemysław Biecek. Models in the wild: On corruption robustness of neural nlp systems. In *Neural Information Processing: 26th International Conference, ICONIP 2019, Sydney, NSW, Australia, December 12–15, 2019, Proceedings, Part III 26*, pages 235–247. Springer, 2019.

[60] Weijie Su, Xizhou Zhu, Yue Cao, Bin Li, Lewei Lu, Furu Wei, and Jifeng Dai. Vl-bert: Pre-training of generic visual-linguistic representations. *arXiv preprint arXiv:1908.08530*, 2019.

[61] Alane Suhr, Stephanie Zhou, Ally Zhang, Iris Zhang, Huajun Bai, and Yoav Artzi. A corpus for reasoning about natural language grounded in photographs. *arXiv preprint arXiv:1811.00491*, 2018.

[62] Yi-Lin Sung, Jaemin Cho, and Mohit Bansal. Vl-adapter: Parameter-efficient transfer learning for vision-and-language tasks. In *Proceedings of the IEEE/CVF Conference on Computer Vision and Pattern Recognition*, pages 5227–5237, 2022.

[63] Yi-Lin Sung, Varun Nair, and Colin A Raffel. Training neural networks with fixed sparse masks. *Advances in Neural Information Processing Systems*, 34:24193–24205, 2021.

[64] Hao Tan and Mohit Bansal. Lxmert: Learning cross-modality encoder representations from transformers. *arXiv preprint arXiv:1908.07490*, 2019.

[65] Yapeng Tian and Chenliang Xu. Can audio-visual integration strengthen robustness under multimodal attacks? In *Proceedings of the IEEE/CVF Conference on Computer Vision and Pattern Recognition*, pages 5601–5611, 2021.

[66] Maria Tsimpoukelli, Jacob L Menick, Serkan Cabi, SM Eslami, Oriol Vinyals, and Felix Hill. Multimodal few-shot learning with frozen language models. *Advances in Neural Information Processing Systems*, 34:200–212, 2021.

[67] James Tu, Huichen Li, Xinchen Yan, Mengye Ren, Yun Chen, Ming Liang, Eilyan Bitar, Ersin Yumer, and Raquel Urtasun. Exploring adversarial robustness of multi-sensor perception systems in self driving. *arXiv preprint arXiv:2101.06784*, 2021.

[68] Ashish Vaswani, Noam Shazeer, Niki Parmar, Jakob Uszkoreit, Llion Jones, Aidan N Gomez, Łukasz Kaiser, and Illia Polosukhin. Attention is all you need. *Advances in neural information processing systems*, 30, 2017.

[69] Ramakrishna Vedantam, C Lawrence Zitnick, and Devi Parikh. Cider: Consensus-based image description evaluation. In *Proceedings of the IEEE conference on computer vision and pattern recognition*, pages 4566–4575, 2015.

[70] Peng Wang, An Yang, Rui Men, Junyang Lin, Shuai Bai, Zhikang Li, Jianxin Ma, Chang Zhou, Jingren Zhou, and Hongxia Yang. Unifying architectures, tasks, and modalities through a simple sequence-to-sequence learning framework. *arXiv preprint arXiv:2202.03052*, 2022.

[71] Wenhui Wang, Hangbo Bao, Li Dong, Johan Bjorck, Zhiliang Peng, Qiang Liu, Kriti Aggarwal, Owais Khan Mohammed, Saksham Singhal, Subhojit Som, et al. Image as a foreign language: Beit pretraining for all vision and vision-language tasks. *arXiv preprint arXiv:2208.10442*, 2022.

[72] Xiao Wang, Qin Liu, Tao Gui, Qi Zhang, et al. Textflint: Unified multilingual robustness evaluation toolkit for natural language processing. In *Proceedings of the 59th Annual Meeting of the Association for Computational Linguistics and the 11th International Joint Conference on Natural Language Processing: System Demonstrations*, pages 347–355, Online, aug 2021. Association for Computational Linguistics.

[73] Boxi Wu, Jindong Gu, Zhifeng Li, Deng Cai, Xiaofei He, and Wei Liu. Towards efficient adversarial training on vision transformers. In *Computer Vision–ECCV 2022: 17th European Conference, Tel Aviv, Israel, October 23–27, 2022, Proceedings, Part XIII*, pages 307–325. Springer, 2022.

[74] Karren Yang, Wan-Yi Lin, Manash Barman, Filipe Condessa, and Zico Kolter. Defending multimodal fusion models against single-source adversaries. In *Proceedings of the IEEE/CVF Conference on Computer Vision and Pattern Recognition*, pages 3340–3349, 2021.

[75] Chenyu Yi, Siyuan Yang, Haoliang Li, Yap-peng Tan, and Alex Kot. Benchmarking the robustness of spatial-temporal models against corruptions. *arXiv preprint arXiv:2110.06513*, 2021.

[76] Elad Ben Zaken, Shauli Ravfogel, and Yoav Goldberg. Bitfit: Simple parameter-efficient fine-tuning for transformer-based masked language-models. *arXiv preprint arXiv:2106.10199*, 2021.

[77] Yan Zeng, Xinsong Zhang, Hang Li, Jiawei Wang, Jipeng Zhang, and Wangchunshu Zhou. X ^{2}-vlm: All-in-one pre-trained model for vision-language tasks. *arXiv preprint arXiv:2211.12402*, 2022.

[78] Renrui Zhang, Rongyao Fang, Wei Zhang, Peng Gao, Kunchang Li, Jifeng Dai, Yu Qiao, and Hongsheng Li. Tip-adapter: Training-free clip-adapter for better vision-language modeling. *arXiv preprint arXiv:2111.03930*, 2021.

[79] Ce Zhou, Qian Li, Chen Li, Jun Yu, Yixin Liu, Guangjing Wang, Kai Zhang, Cheng Ji, Qiben Yan, Lifang He, et al. A comprehensive survey on pretrained foundation models: A history from bert to chatgpt. *arXiv preprint arXiv:2302.09419*, 2023.

A Corruption Details

A.1 Image Corruption Methods

We have incorporated 20 image corruption methods (Fig. 8) following [26, 4, 53] which can be categorized into 5 categories **noise**, **blur**, **weather**, **digital**, and **extra**. We also introduce 5 levels of severity (Fig. 9) to image corruption methods except for *blank* corruption.

Noise There are 4 different noises used in this study, namely *Impulse, Gaussian, Shot, and Speckle*. *Impulse noise* mimics the corruption caused by bit errors by introducing a mixture of salt and pepper noise, with varying intensities such as 0.03, 0.06, 0.09, 0.17, and 0.27. *Gaussian noise* simulates corruptions due to low-lighting conditions by pixel value normalization and normal noise addition. The intensity of this noise is scaled according to severity, with values of 0.08, 0.12, 0.18, 0.26, and 0.38. *Shot noise* simulates electronic noise caused by discrete light and is also called Poisson noise. *Speckle noise* is an additive noise where larger noise will be added if the original pixel value is larger.

Blur *Zoom blur* is observed when the camera swiftly moves toward an object. It blurs toward the center of the frame. *Defocus blur* occurs when the image is out of focus and its severity is defined by the disk radius convolved over the image ranging from $(3, 0.1), (4, 0.5), (6, 0.5), (8, 0.5), (10, 0.5)$. *Motion blur* occurs when the camera is moving quickly. The blurring effect is created by a kernel with different radius and sigma ranging from $(10, 3), (15, 5), (15, 8), (15, 12), (20, 15)$. *Frosted Glass blur* occurs when the glass of windows or panels frosts. *Gaussian blur* generates blurred pixels by a weighted average of its neighbors. The farther the neighbors are, the lower the weight in the average is.

Digital *JPEG* is a lossy image compression format that converts the original picture to JPEG format with quality ranging from $25, 18, 15, 10, 7$ given different severity. *Contrast* simulates corruptions caused by the lighting conditions and object's color. *Elastic* stretches small image regions for stretching effects. *Spatter* appears when the lens is occluded by rain or mud. *Pixelate* transforms the original images into a small number of large pixels.

Weather *Snow* mimics the visual obstruction caused by precipitation. *Frost* occurs when lenses are covered by ice crystals. *Fog* obscures the object and is rendered by the diamond-square algorithm. *Brightness* adds a bright effect to the image simulating daylight.

Extra we introduce a new corruption method called *blank* that sets all pixel values to 255, i.e. turning the original image into a blank picture.

A.2 Text Corruption Methods

We have included 35 text corruptions methods following [72, 53, 4] which corrupt on 3 levels (e.g. character, word, and sentence level) and can be categorized into 3 main categories, 6 sub-categories.

Character Modification. *Character modification* simulates common mistakes during typing and corrupts the text on a character level and contains 9 methods, namely *OCR*, *Punct*, *Typos*, *Keyboard*, *Spelling Error*, *char random insert*, *char random replace*, *char random swap*, *char random delete*. *OCR* replaces a character based on common Optical Character Recognition (OCR) errors. *Keyboard* substitutes original characters based on keyboard distance.

Text Style Transformation. Methods in the *text style* category modify the text on a sentence level and transform the sentence style to a target one, such as turning the original sentence to *passive, formal, causual*, to *double negative*, and changing the *tense*.

Text Addition. *Text addition* inserts additional words to the original text. *InsertAdv* adds an adverb before each verb. *AppendIrr* adds irrelevant phrases to the original texts. *Random Insert* randomly inserts token `[UNK]` to the original texts.

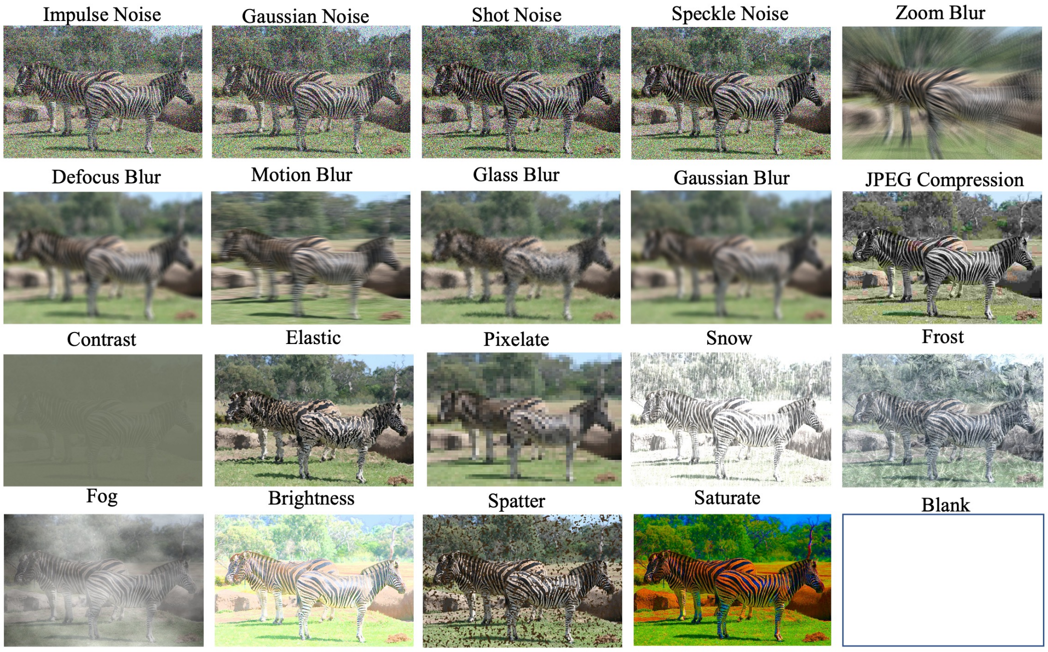

Figure 8: We introduce 20 corruption methods to image data following the methods in [26]. Except for the blank corruption, each type of corruption has five levels of severity. In total, there are 96 different corruptions, as shown in Appendix 3

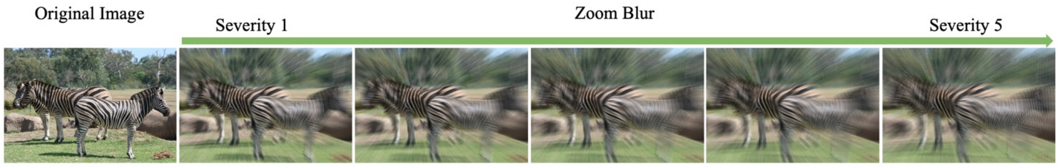

Original text: Does the grass below the zebra appear to be green and short?
Keyboard: Doeq the geass belo! the zebra appear to be green amd short/
OCR: Does the gkass below tbe zebka appear to 6e green and shorl?
Random word insert: Does [UNK] the [UNK] grass below [UNK] the zebra appear to be green and short?

Figure 9: Examples of image and text corruptions. The top row shows an original image from GQA and images corrupted by *zoom blur* with 5 levels of severity. The second row presents text corruptions on the original texts where the red sign indicates the corrupted parts. More examples are shown in supplementary material.

Text Drop based on POS. *Text drop* transforms the text on a word level based on POS tagging [72]. There are methods of dropping nouns (*DropNN*), verbs (*DropVB*), dropping both nouns and verbs (*Drop VB & NN*), dropping random nous and verbs (*Drop Rand NN, Drop Rand VB*), keeping only nouns (*Only NN*), keeping only verbs (*Only VB*), keeping both (*Only NN & VB*).

Text Drop based on Position. According to the word position, there are methods of dropping the first (*Drop First*), dropping the last (*Drop Last*), dropping both the first and the last (*Drop First and Last*), shuffling word order (*Shuffle Order*), and randomly removing words (*Random Delete*).

Text Swap. Under the category of *text swap*, we can replace words randomly or with synonyms by word embedding (*SwapSyn Word Embd*) and WordNet [49] (*SwapSyn WordNet*). We also deploy back translation (*Back Trans*) from [72], which first translates English into French and then translates it back to English. *Randwom Swap* randomly swaps words position.

Table 3: Image Corruption Methods

Category	Corruption Method	Severity
Noise	Impulse	5
	Gaussian	5
	Shot	5
	Speckle	5
Blur	Zoom	5
	Defocus	5
	Motion	5
	Frosted Glass	5
	Gaussian Blur	5
Digital	JPEG	5
	Contrast	5
	Elastic	5
	Saturate	5
	Spatter	5
	Pixelate	5
Weather	Snow	5
	Frost	5
	Fog	5
	Brightness	5
Extra	Blank	1
5 Category	20 Methods	96 Severity

In addition to the above corruptions, Qiu et al. proposed in [53] that we should ensure the corrupted text has the same semantics as the original one to make sure the image-text pairs remain meaningful. We follow this setting and use the same fidelity guarantee mechanism as [53].

B Model Implementations

B.1 CLIP-BART/T5

CLIP-BART/T5 [62], a combination of CLIP and BART/T5, follows VL-T5 [7] which unifies VL tasks to a text-generation problem. Specifically, given a pair of an image x^I and a sentence x^S, e.g. a picture and corresponding question texts in VQA, as the input to the model, CLIP-BART/T5 aims to maximize the agreement between the prediction and text label of M tokens $\mathbf{y} = (y_1, y_2, \ldots, y_M)$. The primary generative model is an encoder-decoder language model, parameterized by θ^L. Visual representation from input images is extracted from a CLIP and a visual projection layer, parameterized by θ^V and $\theta^{V\to L}$ respectively. The concatenation of visual representation and sentence representation is fed into the encoder-decoder language model. The training goal is to minimize the cross-entropy loss [62]:

$$\begin{aligned} & l\left(\boldsymbol{x}^I, \boldsymbol{x}^S, \boldsymbol{y}; \theta^L, \theta^V, \theta^{V\to L}\right) \\ & = \mathrm{CE}\left(f_{\theta^L}\left(\boldsymbol{x}^{V\to L}, \boldsymbol{x}^S\right), \boldsymbol{y}\right) \\ & = -\sum_{i=1}^{M} y_i \log\left(f_{\theta^L}\left(\boldsymbol{x}^{V\to L}, \boldsymbol{x}^S\right)_i\right), \end{aligned} \tag{1}$$

where f_θ means a function parameterized by θ, $\boldsymbol{x}^{V\to L}$ is the projected visual representation.

The unified structure is beneficial to multi-task training where a universal dataset $\mathcal{D}$ from N VL datasets is constructed and used to train the VL model. Under such a scenario, the parameters are optimized by minimizing the averaging loss on $\mathcal{D}$ [62]:

Table 4: Text Corruption Methods

Category	Sub Category	Level	Corruption Method	Severity
Natural	Char Modification	character	OCR	5
		character	Punct	1
		character	Typos	5
		character	Keyboard	5
		character	Spelling Error	5
		character	char random insert	5
		character	char random replace	5
		character	char random swap	5
		character	char random delete	5
	Text Style	sentence	Passive	1
		sentence	Tense	1
		sentence	Formal	1
		sentence	Casual	1
		sentence	Active	1
		sentence	Double Neg	1
	Text Addition	word	InsertAdv	1
		word	Appendlrr	1
		word	Random Insert	5
Synthetic	Drop Text based on POS tag	word	Drop NN	1
		word	Drop Rand NN	1
		word	DropVB	1
		word	Drop VB & NN	1
		word	Only NN	1
		word	Only VB	1
		word	Only NN & VB	1
		word	Drop Rand VB	1
	Positional Drop	word	Drop First	1
		word	Drop Last	1
		word	Drop First and Last	1
		sent	Shuffle Order	1
		word	Random Delete	5
Machine	Text Swap	word	SwapSyn Word Embd	5
		word	SwapSyn WordNet	5
		sentence	Back Trans	1
		word	Random Swap	5
			35 methods	87 levels of severity

$$
\begin{aligned}
&\mathcal{L}\left(\mathcal{D}; \theta^L, \theta^V, \theta^{V\to L}\right) \\
&= \frac{1}{|\mathcal{D}|} \sum_{(\boldsymbol{x}^I, \boldsymbol{x}^S, \boldsymbol{y}) \in \mathcal{D}} l\left(\boldsymbol{x}^I, \boldsymbol{x}^S, \boldsymbol{y}; \theta^L, \theta^V, \theta^{V\to L}\right)
\end{aligned}
\tag{2}
$$

B.2 Adaptation Methods

Full fine-tuning directly updates the whole $\boldsymbol{\theta}$ on $\mathcal{D}$ and becomes prohibitive due to the rapidly growing model size. For instance, simply loading a GPT-3 language model with 175B parameters as the VL model backbone would require 700GB of memory [3]. Therefore, the following more efficient adaptation methods are developed to achieve comparable performance while optimizing only a few parameters.

Prompt-based adaptation modifies the input $\mathbf{x}$ to the model F by either concatenating a trainable prefix (Soft Prompt) [36] or a manually designed prefix [3]. For the given input $\mathbf{x} = \{x_1, \ldots, x_n\}$ with n tokens, the pre-trained model will first form an embedding matrix $\mathbf{X} \in \mathbb{R}^{n\times d}$ where d is the

[3] $(175 \times 10^9) \times 4(\text{bytes}) \times 10^{-9} = 700\text{GB}$

Table 5: We deploy eleven distinct adaptation methods in total.

Type	Method
Full Fine-tuning	Full Fine-tuning
Adapter [29]	Single Adapter Half-shared Adapters Multiple Adapters
Compacter [33]	Single Compacter Multiple Compacter
Hyperformer [46]	Hyperformer
LoRA [30]	Single LoRA Multiple LoRA
Soft Prompt [36]	Single Prompt Multiple Prompts

dimension of the embedding space. Soft-prompts [36] are then represented as a learnable parameter $\mathbf{P} \in \mathbb{R}^{p \times d}$ where p is the length of the prompt. Next, $\mathbf{P}$ is concatenated with the original embedded input $\mathbf{X}$ to form a new single matrix defined as $[\mathbf{P}; \mathbf{X}] \in \mathbb{R}^{(p+n) \times d}$. During adaptation, the model is trained to maximize the probability of the desired output while only updating $\mathbf{P}$.

LoRA [30] also freezes the pre-trained model parameters $\boldsymbol{\theta}$, but it utilizes low-rank decomposition matrices to update gradients. For an intermediate model parameter $\theta_0 \in \mathbb{R}^{d \times k}$, which can be the parameters from one self-attention module in the transformer architecture, its update is represented by a low-rank decomposition as shown in Formula 3. θ_0 is frozen, whereas B and A contain trainable parameters while adapting.

$$\theta_0 + \Delta\theta = \theta_0 + BA, B \in \mathbb{R}^{d \times r}, A \in \mathbb{R}^{r \times k}, r \ll min(d, k). \tag{3}$$

Adapter-based adaptation inserts small modules between parameters in $\boldsymbol{\theta}$ and modifies the intermediate learning process. Variants of adapter-based methods differ in the insertion manner. Adapters[29] consists of a pair of downsampling and upsampling layers and a residual connection. Suppose the original input to an intermediate layer θ_0 in model $\boldsymbol{\theta}$ is $\mathbf{x}_0 \in \mathbb{R}^{d_0}$, adapters insert a downsampling layer $\theta^D \in \mathbb{R}^{d_0 \times d_1}$ and an upsampling layer $\theta^U \in \mathbb{R}^{d_1 \times d_0}$ where d_0, d_1 are dimensions of the hidden embeddings. The output after injecting adapters is defined in Formula 4 where $\sigma(\cdot)$ is an activation function such as GELU [27].

$$h = f_{\theta^U}\left(\sigma\left(f_{\theta^D}(\mathbf{x}_0)\right)\right) + \mathbf{x}_0 \tag{4}$$

Compacter [33] is based on the mechanism of adapters [29], but it utilizes matrix decomposition and parameter sharing to further reduce redundant parameters in adapters. It introduces *parameterized hypercomplex multiplication* (PHM) layers (Formula 5), which decompose the layer in the adapter by Kronecker products. Compacter also shares the parameter of A_i across all layers and decomposes B_i even further with low-rank decomposition. However, as found in [62], such sharing and further decomposition severely decreases the VL performance. In our study, we only use PHM layers.

$$\theta^D = \sum_{i=1}^{k} A_i \otimes B_i, A_i \in \mathbb{R}^{k \times k}, B_i \in \mathbb{R}^{\frac{d_0}{k} \times \frac{d_1}{k}} \tag{5}$$

Hyperformer [46] also aims to reduce redundant parameters in adapters. It relies on a hyper-network that is shared across tasks to generate the weights in adapters given a task index and a layer index. The hyper-network maintains learnable embeddings for each task and each layer. For N_T tasks and N_L layers, the d_e-dimensional embeddings can be denoted as $\boldsymbol{t}_1, \ldots, \boldsymbol{t}_{N_T} \in \mathbb{R}^{d_e}$; $\boldsymbol{l}_1, \ldots, \boldsymbol{l}_{N_L} \in \mathbb{R}^{d_e}$. The Hyperformer consists of a task projector $\theta^T \in \mathbb{R}^{(d_e + d_e) \times d_p}$ and a hyper-network $\theta^H \in \mathbb{R}^{d_p \times (d_0 \times d_1 + d_1 \times d_0)}$, and generates an adapter's weights in the i^{th} layer for the j^{th} task following Formula 6.

$$\left[\theta^D, \theta^U\right] = f_{\theta^H}\left(f_{\theta^T}\left([\boldsymbol{t}_j, \boldsymbol{l}_i]\right)\right) \tag{6}$$

Adaptation shared over tasks is inspired by Hyperformer and proposed in [62] which aims to exploit similar information shared across multiple tasks and to reduce redundant parameters. For vanilla adapters in a multi-task setting with N_T tasks, the collection of all inserted adapter modules can be denoted as $\Theta = \{\Theta^D, \Theta^U\}$ where Θ^D (Θ^U) stands for the subset of downsampling (upsampling) layers in adapters. The straightforward application is to train the adaptation modules per task, so we have independent $\{\Theta_i^D, \Theta_i^U\}$ for the i^{th} task, dubbed as **Multiple Adapters**. The same goes for other adaptation methods. By training one prompt, low-rank weights, and compacter layer for each task, we obtain **Multiple Prompts, Multiple LoRA**, and **Multiple Compacter** respectively. We can also train only one set of adapter layers for all tasks, and we have **Single Adapter** where $\Theta_i^D = \Theta_j^D$ and $\Theta_i^U = \Theta_j^U, i \neq j$. Also, if we use the same prompts, low-rank weights, and compacter layers, we have **Single Prompt, Single LoRA**, and **Single Compacter** respectively. For adapters, we can make parts of the weights shareable by making $\Theta_i^D = \Theta_j^U, i \neq j$ and. In this way, the task-specific information of i^{th} can still be learned by the rest Θ_i^U. Such sharing mechanism is called **half-shared adapter**. Lastly, Hyperformer already shares information from multiple tasks and therefore does not have such extensions.

B.3 Training and Evaluation

We follow the same experimental and hyperparameter settings as [62]. CLIP-ResNet101 is the vision encoder that takes the resized 224 × 224 images as input. The 7 × 7 gird features in the last convolutional layer are extracted as visual features and are downsampled to 6 × 6 by adaptive maximum pooling. BART$_{base}$ and T5$_{base}$ are both studied in this work as encoder-decoder language models. During training, AdamW is the optimizer along with a linear decay scheduler. Models are trained for 20 epochs, and the learning rate increases from 0 to the highest learning rate in the first 2 epochs. Training batch sizes are set as 500 and 250 for CLIP-BART and CLIP-T5 respectively. Models are trained in a multi-task setting where the training dataset includes all training split from 4 VL datasets. After training, we first evaluate the clean performance. Specifically, accuracy on the Karpathy-test split is evaluated for VQAv2. For GQA, accuracy on the test-dev split is evaluated, and accuracy on the test-P split is used for NLVR^2. In image captioning, we use CIDEr [69] on the Karpathy-test split. Then, we evaluate the corrupted performance on the corresponding corrupted test split from each dataset and calculate the relative robustness. All the training and evaluations are conducted on LRZ AI Systems at the Leibniz Supercomputing Centre of the Bavarian Academy of Sciences and Humanities.

C Limitations

The limitations of this work mainly include 1) the adoption of simulated noise instead of real-world data due to the difficulty of obtaining real-world corruptions, 2) the analysis is on a limited number of multimodal models due to the availability of usable code, model weights, and the massive experiments, 3) the experiments require heavy GPU usage to pre-train vision-language models.

D Licensing

All the models and datasets used in this study are publicly available. The code for model VL-T5(BART) and CLIP-T5(BART) have the MIT License and the code for Hyperformer and Soft Prompt has the Apache 2.0 License. Our benchmark datasets are built upon 4 well-known and publicly available VL datasets, namely VQAv2 [20], GQA [31], NLVR^2 [61], and MSCOCO [5]. We also publicize our benchmark datasets, corruption codes, and benchmark codes under MIT License.

E Impact

From our understanding, there are no negative societal impacts of our study. This study aims to investigate the robustness of multimodal adaptation methods and facilitate future research and real-world applications.